Scientific Visualization, 2023, volume 15, number 5, pages 136 - 148, DOI: 10.26583/sv.15.5.11

The Spectrum of Supersonic Flow Around an Aircraft with Control Brake Shields

S.I. Gerasimov[1,A,B,C], A.A. Glukhov[2,A], V.A. Kikeev[3,C], I.Yu. Smirnov[4,A], K.V. Totyshev[5,A]

[A] Russian Federal Nuclear Center — All-Russian Research Institute of Experimental Physics, Sarov, Nizhny Novgorod Region, Russia
[B] Sarov Institute of Physics and Technology of the National Research Nuclear University "MEPhI", Sarov, Nizhny Novgorod region, Russia
[C] Institute for Problems in Mechanical Engineering of the Russian Academy of Sciences, Nizhny Novgorod, Russia

[1] ORCID: 0000-0002-6850-0816, s.i.gerasimov@mail.ru
[2] ORCID: 0000-0003-4470-6518, glukhow.a@yandex.ru
[3] ORCID: 0000-0002- 2040-2045, vkikeev@mail.ru
[4] ORCID: 0000-0002- 5419-5312, smirnovig@yandex.ru
[5] ORCID: 0000-0002- 6232-505X, totyshev@bk.ru

Abstract

The article presents the results of the study of the spatial flow pattern of the aircraft model, the study of the flow structure near the surface of the aircraft by experimental and numerical methods. Comparative materials for visualizing flows around a conical model with a stern control body – a flat end shield during supersonic flight in atmospheric pressure air are presented. The difference from the qualitative flow pattern according to experimental spectra at M≈4 and M≈5.5 lies in the presence, in addition to the formation of a breakaway flow zone in front of the shield, an oblique jump of the seal (from the point of separation of the flow) and a more intense direct jump of the seal, the possibility of the appearance of a flow separation zone induced by the shield on the side of the model surface opposite the shield, with the formation of an oblique jump of the seal. The efficiency of increasing the number of brake shields installed on the cylindrical-conical model is considered. The results of measurements of the dependence of the increments of the drag coefficient of the tested models on the area of the shields are presented.

Keywords: aeroballistic experiment, aircraft, flow, seal jump, drag, cylindrical-conical model.

The use of photoregistration in an aeroballistic experiment makes it possible to obtain high-quality shadow photographs of the flow spectra, which make it possible to study the flow structures near the surface of the aircraft or its model [1-10]. The study of the spatial flow pattern by reversed experiment and numerical calculation does not guarantee the detection of all possible effects detected while observing dynamic similarity, which can provide a direct aeroballistic experience with shooting a model of an aircraft (AC) into free flight. Thus, according to the theoretical scheme, when a supersonic flow flows around the shield 6 (Fig. 1), located on the lateral conical surface of 2 aircraft, a spatial shock of compaction 5 occurs, which in turn forms a zone of circulation flow 4, bounded by the separation line 7 and the jump 3 [11].

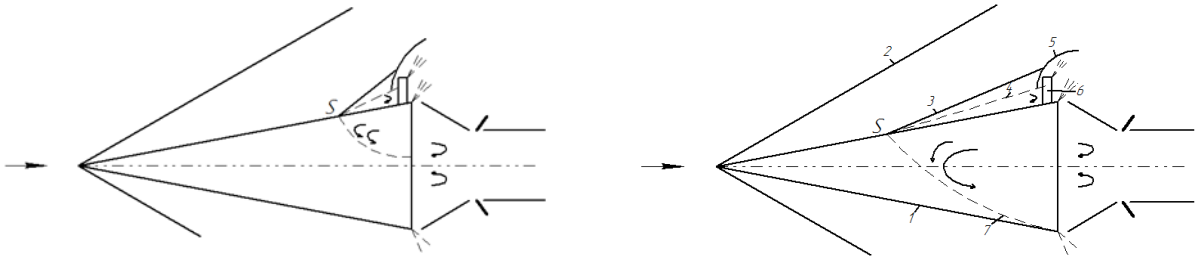

a b

Fig.1. Flow diagram during the flow around the aft shield

The separation of the flow in front of the shield can be laminar (Fig.1,b), transient or turbulent (Fig.1,a), which manifests itself in the form of a significant or small-sized separation zone and small or large flow separation angles (for laminar or turbulent separation, respectively). Consequently, the flow pattern is affected by the roughness of the lateral surface, as well as the relative radius of blunting of the cone and the angle of attack.

1.1. Consider what gives the calculation of a blunted cone with a flat end control panel. A version of the LOGOS engineering software package was used for computer modeling [12]. During the simulation, aerodynamic forces and moments acting on the streamlined surface of the model were determined. All parameters of the flowing gas in the calculated volume are obtained - pressure fields, densities, temperatures, velocities. The three-dimensional calculation of the process of external flow of models by a supersonic flow of compressible gas was carried out taking into account the corresponding boundary conditions on the surface of the model and on the walls of the computational domain. The complete Reynolds-averaged Navier-Stoks equations were solved, supplemented by the equations of kinetic energy transfer of turbulence and its dissipation, formulated in the framework of a two-parameter k-ε turbulence model. At the same time, the transition of a laminar boundary layer to a turbulent one, as well as directly laminar and turbulent boundary layers, are modeled using two-scale wall functions that provide high accuracy and versatility. The appropriate calculation method is selected automatically depending on the calculated grid, two options for calculating the boundary layer depending on the flow parameters are implemented — the "thick boundary layer" model for calculating boundary layers on a detailed grid, and the "thin boundary layer" model for calculating on a coarse grid. It should be noted that in many problems, both approaches allow us to obtain a solution acceptable in accuracy on a rather coarse grid. The range of the considered initial flow velocities was 2 - 6 M. The flow of the model was carried out at the axial direction of the initial flow velocity, that is, at zero angle of attack, as well as at angles of attack -2, 2, 5 and 10 °. For air, the equation of state of a perfect gas was used.

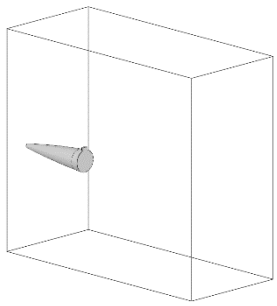

Fig. 2. The computational domain used, constructed taking into account the symmetry conditions.

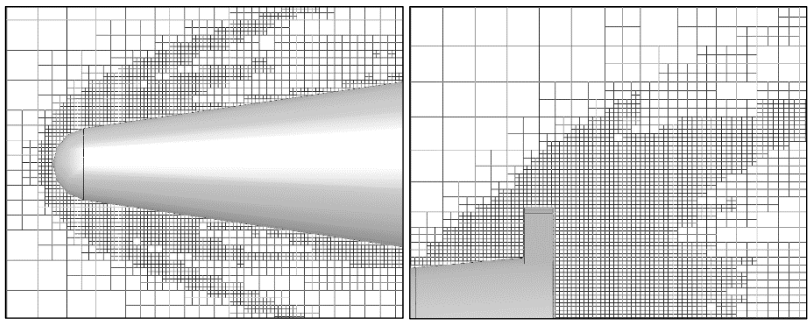

Fig.3. Fragments of a counting grid adapted after 3520 iterations near the bow and stern parts of the model for flow around with an initial velocity of M = 6.

The studied model was characterized by a base diameter of 60 mm and a length of 215.7 mm. The relative area of the control panel was 0.040 of the base area. The dimensions of the calculated domain, taking into account the symmetry, were 68×60×30 cm. The domain with the model located in it (half of the model) is shown in Fig. 2. The original grid consisted of 209524 cells, and the corresponding adapted grids for M = 2-6 consisted of 397544, 589365, 791238, 984648 and 1237320 cells. In Fig. 3, fragments of the adapted grid for flow conditions with an initial velocity of M = 6 are shown on an enlarged scale.

In the process of calculation, the full domain fields were determined for all parameters of the flowing gas, including the distribution on the surface of the model, and the values of all the necessary aerodynamic characteristics of the model were given. In particular, for different initial flow velocities and the five angles of attack considered, the resistance coefficients in the direction of the x and y axes (Cx, Cy) and the moment coefficients relative to the z axis (m_z) were determined. When determining the values of the coefficients, the value of the total area of the maximum cross-section of the model, taking into account the shield, was used.

The results obtained at different angles of attack are shown in Fig. 4-11. Figures 4-6 show the nature of the change in the values of the coefficients C_x, C_y and m_z with an increase in the number of iterations, that is, the nature of their convergence. The calculation results for M = 2, 3, 4, 5 and 6 are indicated respectively by rhombuses, squares, triangles, circles and markers in the shape of the letter Ж. Fig. 7a shows the pressure field for the initial flow velocity M = 2. The pressure range used for visualization is 0 - 600 kPa here, the width of the monochromatic bands in the upper image corresponds to a value of 2.4 kPa. Figure 7b shows the density field for the initial flow velocity M = 2. The density range used for visualization is 0 - 5 kg/m³ here, the width of the monochromatic bands in the upper image corresponds to a value of 20 g/m³. Figure 7b shows the temperature field for the initial flow velocity M = 2. The temperature range used for visualization is 200-600 K here, the width of the monochromatic bands in the right image corresponds to a value of 1.6 K. The results obtained at angles of attack -2, 2, 5, and 10° are shown in Fig. 8-11. The width of the monochromatic bands in the upper image of Fig. 11b corresponds to a value of 2.0 K.

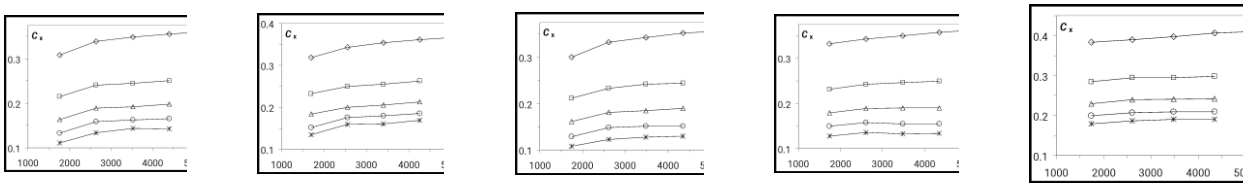

a *b* *c* *d* *e*

Fig. 4. The change in the values of the C_x coefficients with an increase in the number of iterations for the angles of attack α = 0° (a), -2° (b), 2° (c),5° (d), 10 ° (d) and the initial flow velocity M = 2-6.

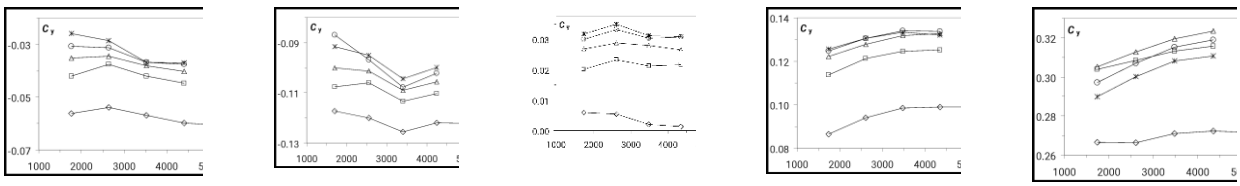

a *b* *c* *d* *e*

Fig. 5. The change in the values of the C_y coefficients with an increase in the number of iterations for the angles of attack α = 0° (a), -2° (b), 2° (c),5° (d), 10 ° (d) and the initial flow velocity M = 2-6.

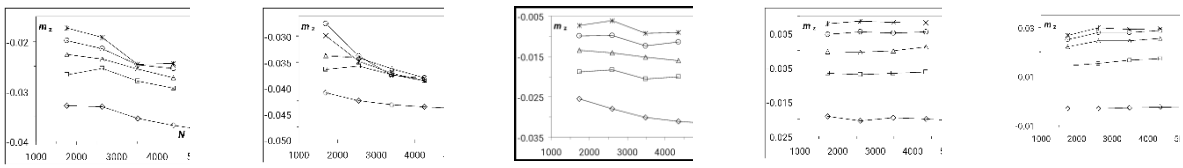

a *b* *c* *d* *e*

Fig. 6. The change in the values of the coefficients mz with an increase in the number of iterations for the angles of attack α = 0° (a), -2° (b), 2° (c),5° (d), 10 ° (d) and the initial flow velocity M = 2-6.

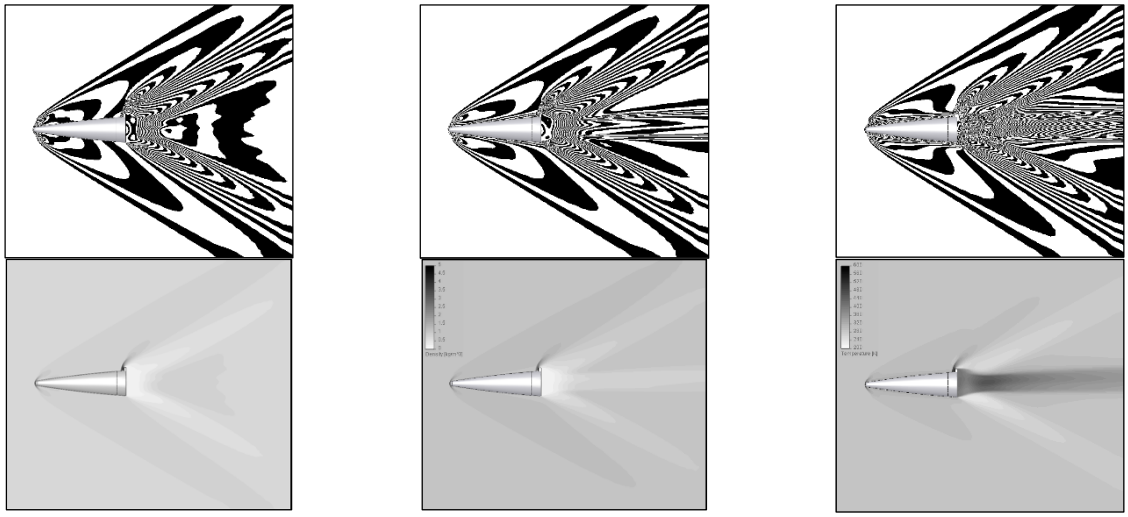

a b c

Fig.7. Pressure fields (a), density (b), temperature (c) for zero angle of attack and initial flow velocity M = 2.

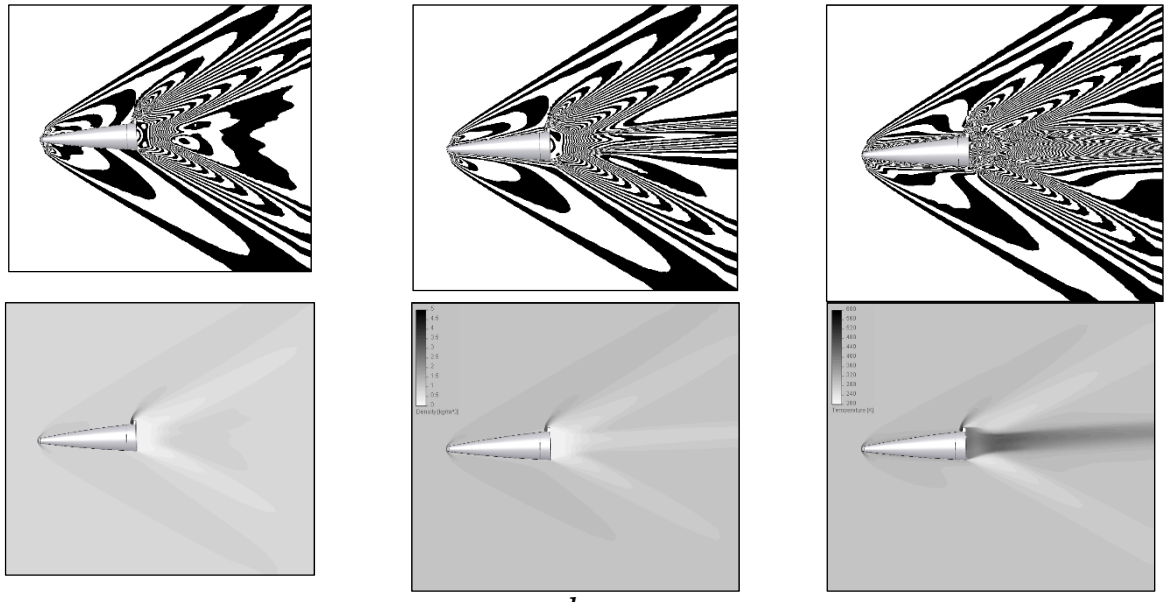

a *b* *c*

Fig. 8. Pressure fields (a), density (b), temperature (c) for the angle of attack α = -2 ° and the initial flow velocity M = 2.

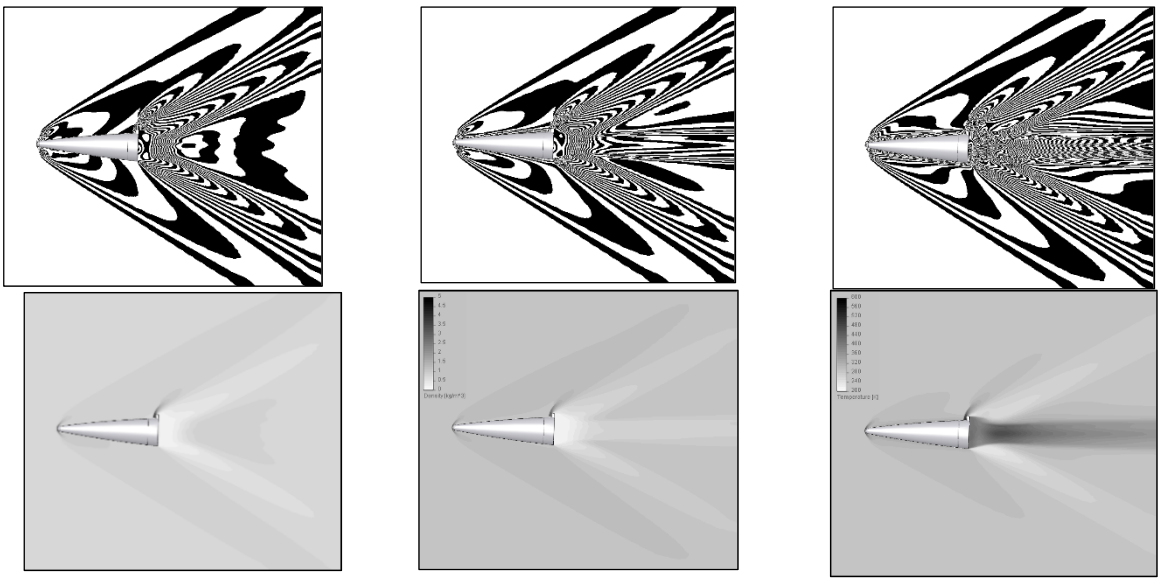

a b c

Fig. 9. Pressure fields (a), density (b), temperature (c) for the angle of attack α = 2 ° and the initial flow velocity M = 2.

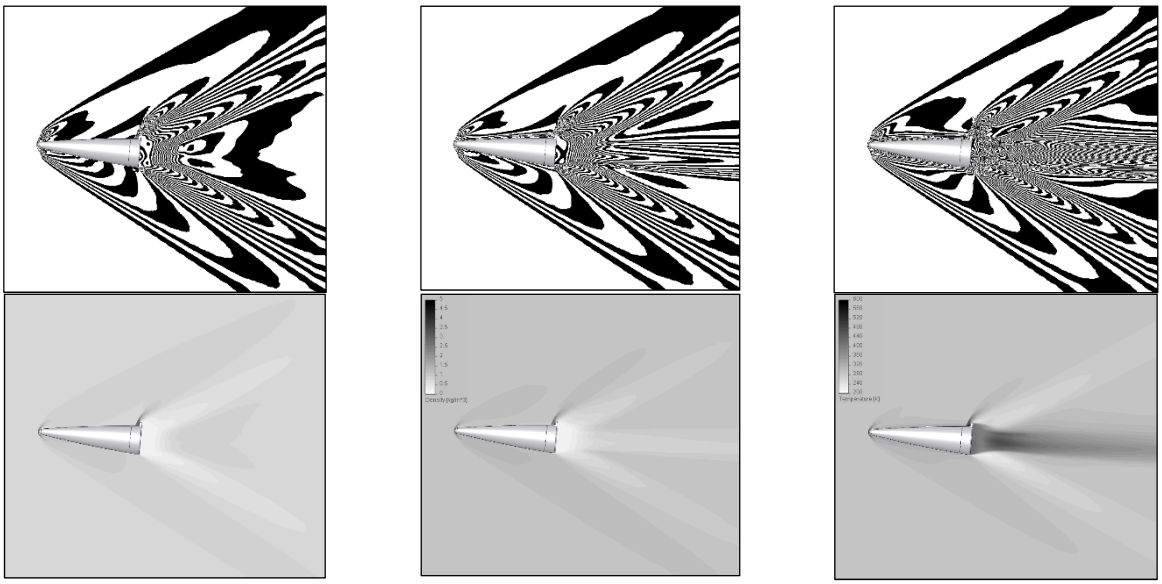

a b c

Fig. 10. Pressure fields (a), density (b), temperature (c) for the angle of attack α = 5 ° and the initial flow velocity M = 2.

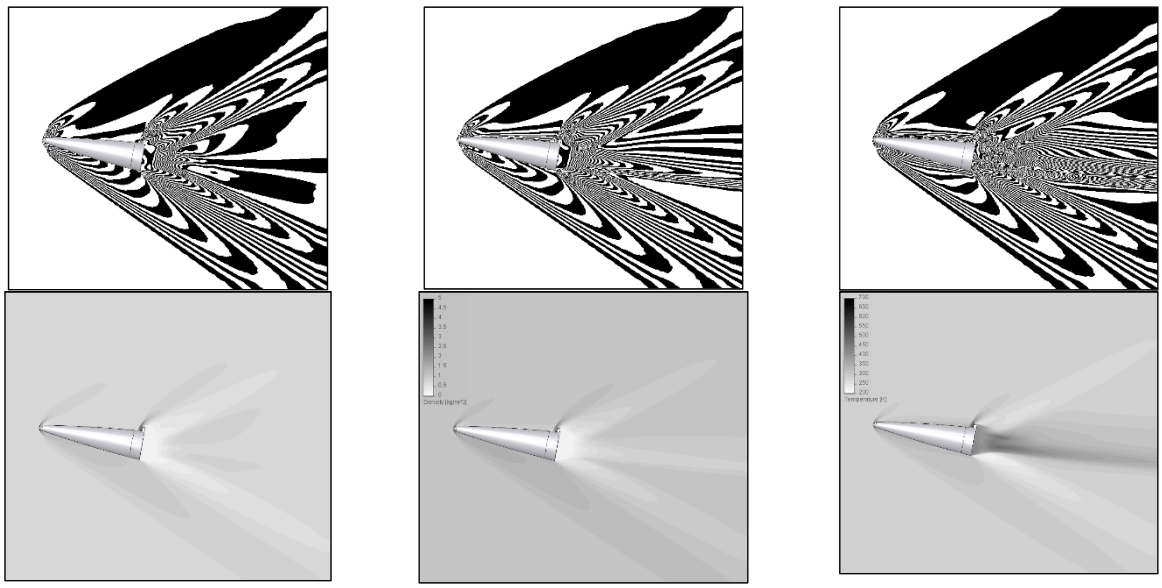

a *b* *c*

Fig. 11. Pressure fields (a), density (b), temperature (c) for the angle of attack α = 10° and the initial flow velocity M = 2.

1.2. Based on the calculated estimates, experiments were carried out in an aeroballistic dash [13], where the dynamics of the flight of a model with a shield control was studied. A model similar to the one discussed above, placed in a split pallet with the shield facing down, was fired from a powder ballistic installation with speeds in the range M = 4-5.5.

The movement of the model is characterized by significant radial deviations relative to the main aiming line of the shooting range in Y and Z (from ≈ 0 m at the beginning of the measuring section to 2.5 m at the end) and the presence of large balancing angles of attack. At the same time, fluctuations in the angle of attack are attenuated. The rotation of the models relative to the longitudinal axis (according to γ) due to the twist in the barrel of the ballistic installation (the appearance of the initial angular velocity of rotation of the model relative to the longitudinal axis ωx0 when the aircraft moves in the barrel channel), occurred clockwise in the direction of movement and led to a change by an amount from 100 to 1050 when moving on the measuring section of the shooting range.

We note significant nonlinear effects in the aerodynamic characteristics of the aircraft due to the presence of unstable unsteady areas in the zone adjacent to the shield at large angles of attack, as well as their dependence on the aerodynamic angle of roll, which led to the appearance of a systematic component depending on the discrepancies between the calculated and experimental values of θ and ψ (pitch and yaw) with good compliance calculated and experimental values of the balancing angle α_{bal}.

The difference from the qualitative flow pattern (Fig.1) according to experimental spectra at M≈4 and M≈5.5 is the presence, in addition to the formation of a breakaway flow zone in front of the shield, an oblique shock of compaction (from the point of flow separation) and a more intense direct shock of compaction, of the possibility of a shield-induced flow separation zone on the surface side 12). Here and further, the shadow spectra are shown reflected vertically by 180° – the shield is up, and in the experiments the model flew with the shield down. The vertical line in the pictures is a vertical plumb line; the horizontal line is the border of two separate films in the cassette.

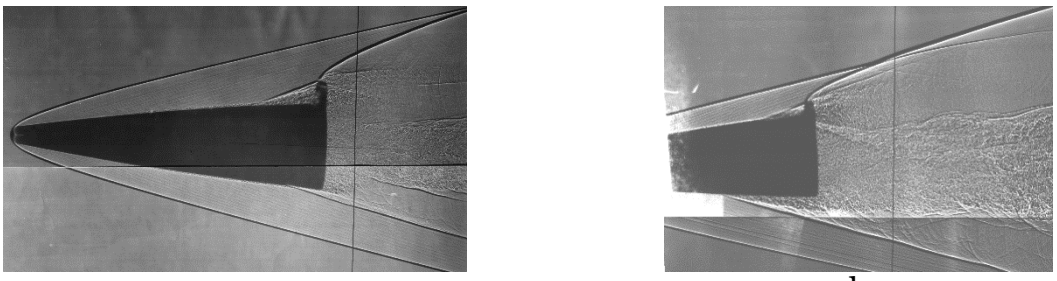

a b

Fig. 12. Shadow spectra of the flow around a model with a flat end shield at V ≈ 1715 m/s, ϑ≈ - 1°,γ = - 160°(a); V≈ 1935 m/s, ϑ≈ 4°, γ= -145° (b)

The size of the tear-off zone depends on the magnitude of the angle of attack and the angle of orientation of the shield relative to the plane of resistance. At an angle of attack close to 0°, the front boundary of the separation zone covers the entire lateral surface of the research object (OI) adjacent to the bottom end and closes on the opposite side near the bottom cut by ℓ = 1.6 (distance from the separation point S to the shield l / h) from it (Fig.12 a). When the shield is located on the leeward side of the model surface, with an increase in the angle of attack, the size of the tear-off zone decreases, and its boundary at angles of attack α ≤ -2° does not close on the windward side of the model surface (Fig.13). When the shield is located on the windward side of the model surface, with an increase in the angle of attack, the size of the tear-off zone increases, and its boundary on the leeward side of the surface moves to the toe of the model and at an angle of attack of ≈4° is separated from this cut by an amount of ℓ = 4.4 (Fig.12 b).

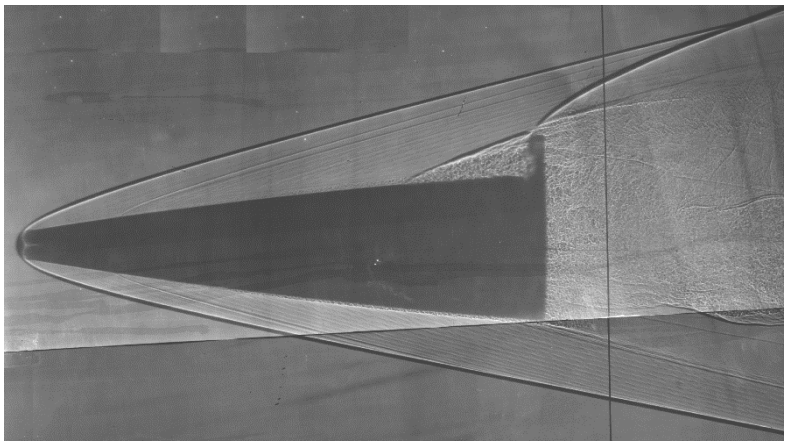

Fig. 13. Shadow spectra of the flow around a model with a flat end shield at V ≈ 1937 m/s, ϑ - 2,5°,γ = - 191°.

2. Since the shield controls installed on this slice demonstrate efficiency when braking the model, it is of interest to consider the feasibility of increasing them. It is of interest how much more complicated the flow spectrum near the aft part of the model is now and whether it is possible to evaluate the effectiveness of changing the air resistance force (drag force coefficient) from the resulting shadow picture. As an object of testing during experiments in the aeroballistic dash, models of cylindrical-conical aircraft without shields were used - variant "N", with twenty evenly spaced brake shields of size h = 0.0917, b = 0.117 - variant "20sh", with four brake shields of size h - b =0.0983 - variant "4sh1" and with four brake shields of size h =b = 0.1683 - option "4sh2". Photos of the models are shown in Fig. 14.

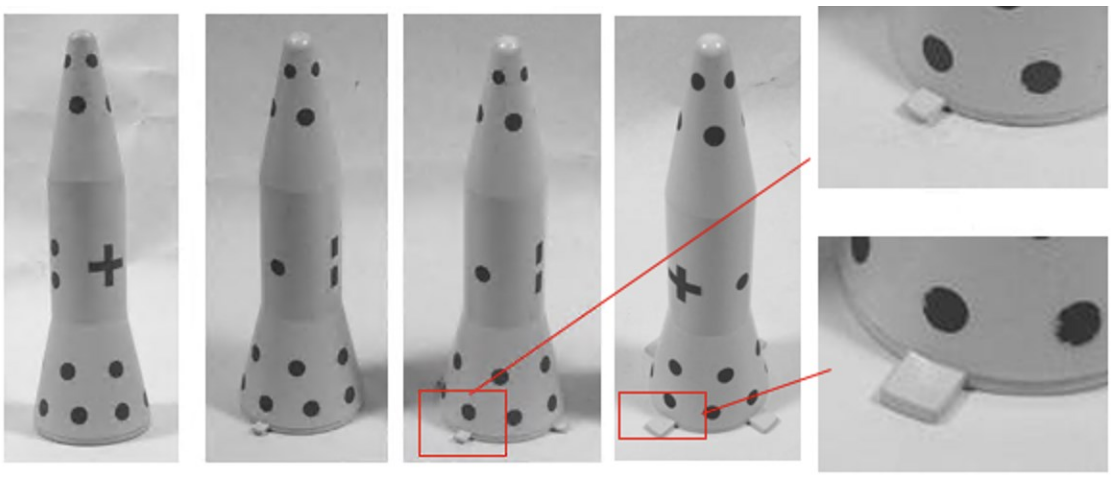

Variant "N" Variant "N + 1sh1" Variant "N + 4sh1" Variant "N + 4sh2" shields

Fig. 14. Photos of models

As a result of aeroballistic tests of models with and without shields, shadow spectra of the flow of models at Mach number were obtained. The sufficiently high quality of shadow spectra for the tested model variants allows us to analyze some features in the flow of models with shield controls. Thus, the shadow spectra of the flow around the aft part of the models have a characteristic appearance for bodies with a conical skirt, in the transition zone to which there is a surge of compaction. The installation of the shields leads to the formation of separation flow zones in front of them. The flow around the shields occurs with the formation of a surge of compaction in front of them.

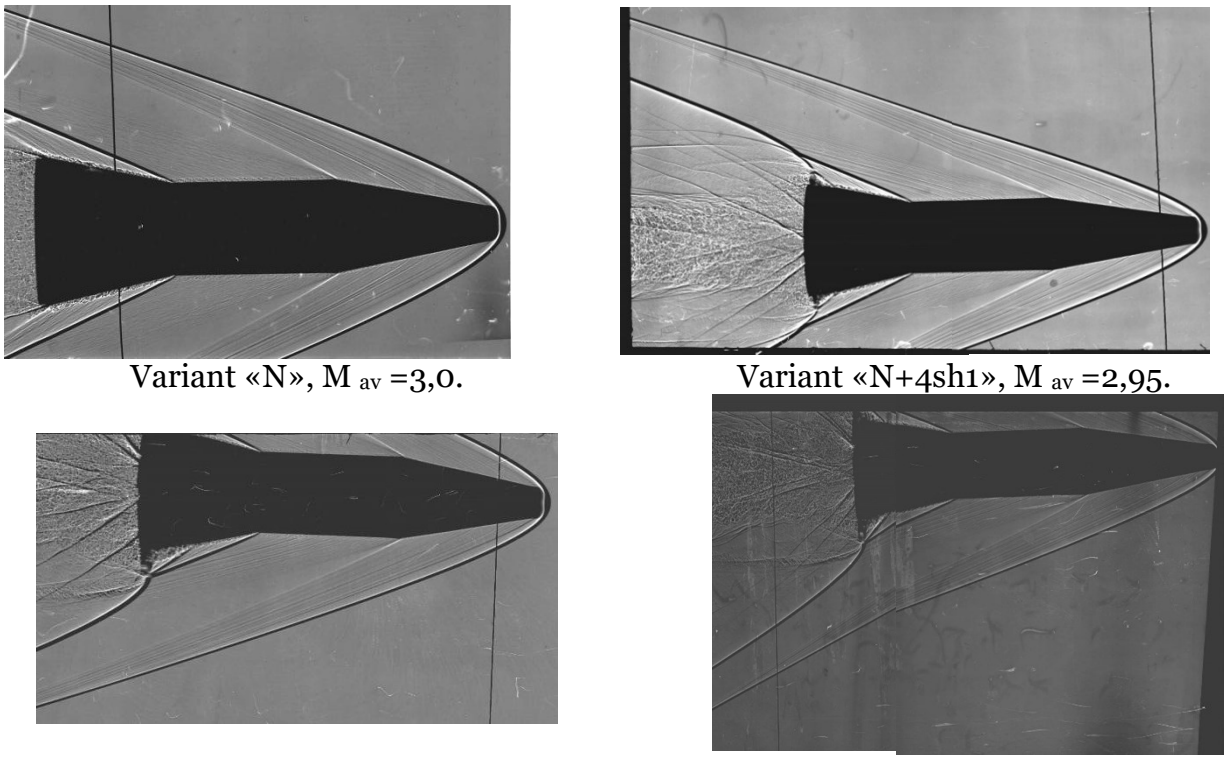

Variant «N», M_{av} =3,0. Variant «N+4sh1», M_{av} =2,95.

Variant «N+4sh1», M_{av} =2,95. Variant «N+4sh2», M_{av} =2,85.

Fig. 15. Flow spectra of the basic model and the model with 4 brake shields.

The coefficients of full and bottom resistance $C_{x\Sigma}$ and C_{xb} models without a shield at $\alpha=0^{\circ}$ decrease with a change in the Mach number from $M_{\infty}=3$ to $M_{\infty}=4$ and increase with an increase in the angle of attack α . The installation of shields, especially large shields,

leads to an increase in the coefficient of longitudinal force $C_{x\Sigma}$. The relative bottom pressure P_b in the absence of a shield decreases with an increase in the Mach number in the studied range $M_\infty = 3 \ldots 4$ and decreases in the angle of attack α . Theoretically, when the shield is located on the windward side of the model ($\alpha = -10°$), an extensive zone of separation flow appears in front of it, bounded on the body by a drain line on which the current lines touch inside and outside the separation zone. At the angle of attack $\alpha = 0°$, the tear-off zone remains very large. When the shield is positioned on the leeward side of the body (which corresponds to the movement of the model at the balancing angle of attack), the role of the separation zone remains significant – (see Fig. 15). The position of the flow separation point was located in the ranges $l_s \approx (2\text{-}4)h$ (see Fig. 16).

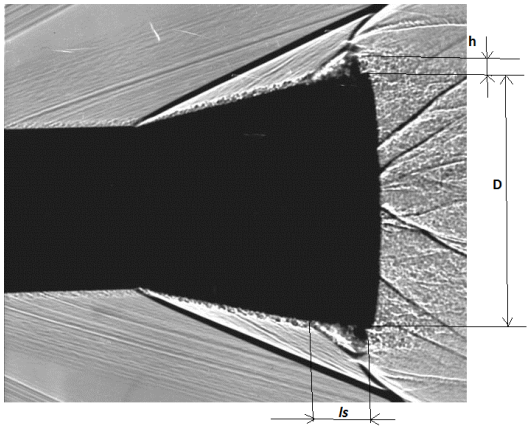

Fig. 16 – Bottom section, h – height of the shield, D – diameter of the midsection.

According to estimates, the gas-dynamic parameters on the surface of the model remain almost constant along the length of its conical part from the shield to $l \leq 0.7D$, when the influence of the cylindrical part of the object becomes noticeable; the position of the separation point l_s the considered range $l_s \approx (2\text{-}4)h$ does not have a noticeable effect on the change in the aerodynamic characteristics of the model due to the installation of the shield.

3. An increase in the number of brake shields to increase the drag coefficient due to the "maximum" possible number of brake shields on the bottom section was considered on the example of a model with twenty evenly spaced brake shields of size h = 0.0917, b = 0.117 - variant "N-20sh".

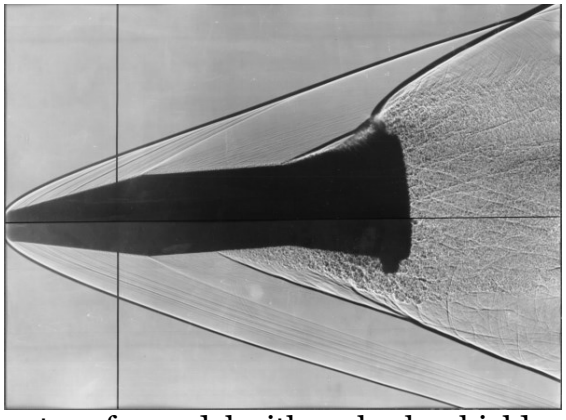

Fig. 17. Flow spectra of a model with 20 brake shields at V≈1440 m/s.

It follows from the results of aeroballistic tests that the presence of twenty evenly spaced brake shields (variant "N20sh") leads to an increase in the coefficient of drag force by 2.5 times (by $\Delta C\tau = 0.407$) at M = 3.

However, with such a number and configuration of shields, a tear-off zone is formed on the surface of the model, the front boundary of which is located far upstream from the

shields on the cylindrical part of the surface of the model (Fig. 17). At the same time, the movement of the models acquires a complex, pronounced inharmonic character of oscillations at pitch angles (θ), yaw (ψ), and in conditions of unsteady flow, this zone causes self-oscillations of the model with an increasing amplitude of oscillations at the corners (Fig. 18).

At the same time, with a smaller number of shields (a greater distance between them in the circumferential direction), the flow pattern of the models is significantly different - the separation zone is localized in the vicinity of each shield (Fig. 15). And from the point of view of increasing the Cτ coefficient, such shields are more effective: for example, four shields with a relative area of 0.144 (option "4Nsh2"), i.e. almost 2 times smaller than the area of 20 shields (option "N20sh"), lead to an increase in Cτ by about 2.1 times. At the same time, there is no phenomenon of "self-oscillation", i.e. stabilization (damping of oscillations) of the models occurs at the corners (Fig. 19).

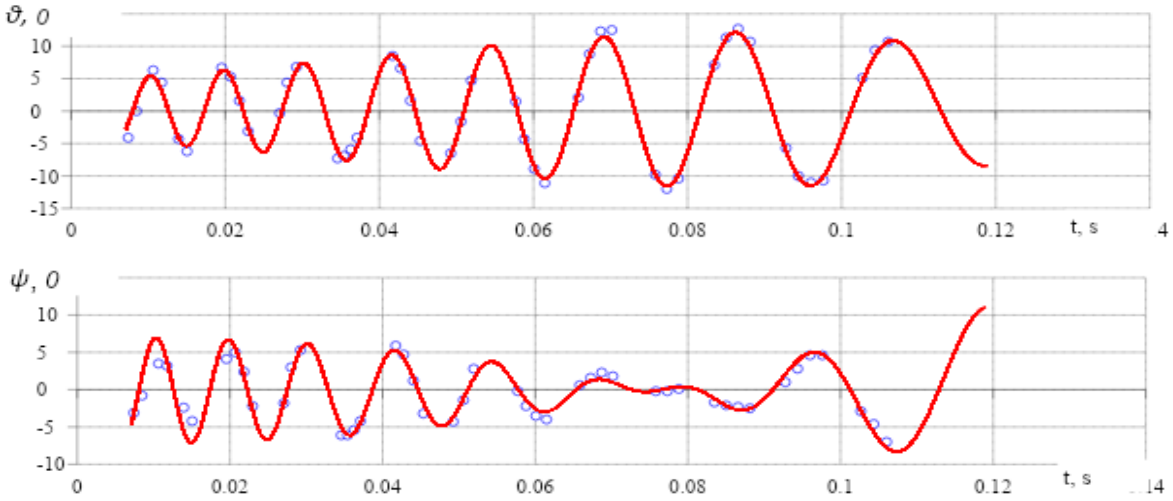

а) test 1

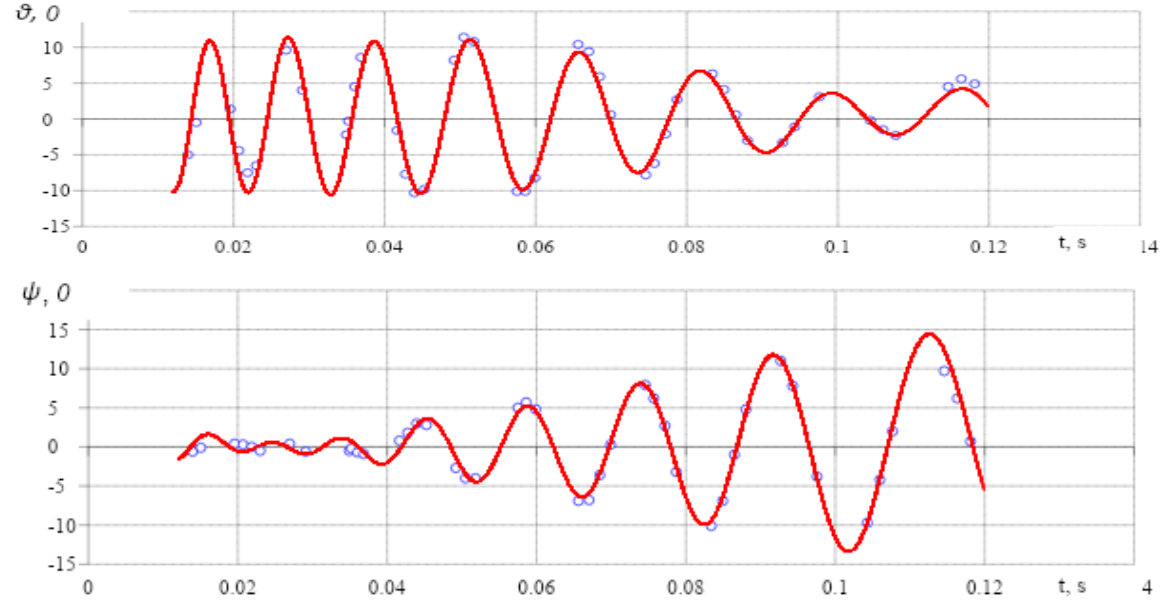

б) test 2

Fig. 18. Dependences of angles and in experiments with the model of the “N20sh” variant (o - test, — calculation).

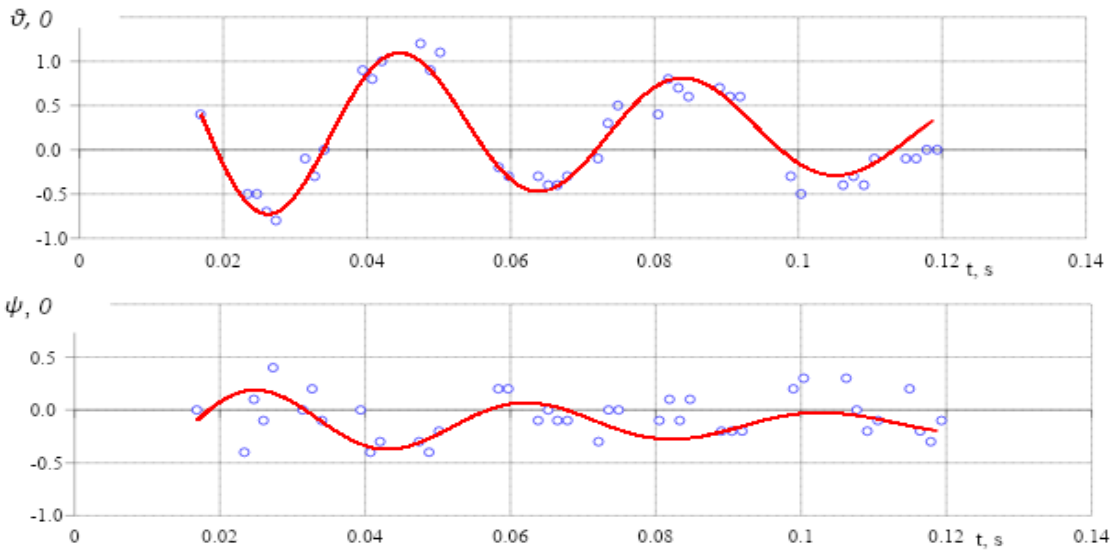

Fig.19. The dependence of the angles ϑ(t) and ψ in the experiment with the model of the variant "4NSH2" (o - test, — calculation).

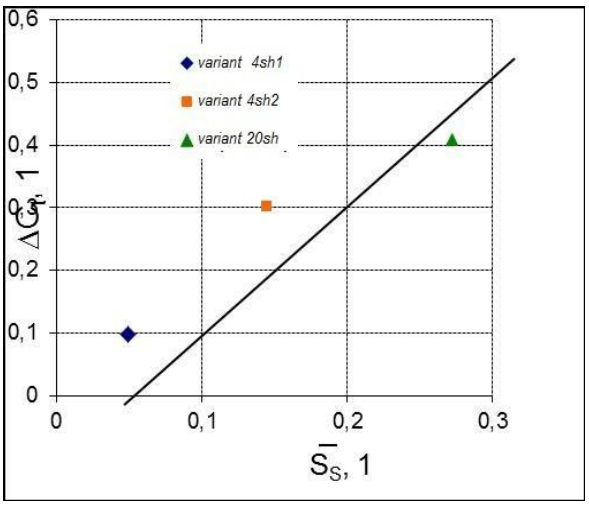

Fig. 20. Dependence of ΔCτ on the area of the shields

Figure 20 shows the dependences of the increments of the drag coefficient ΔCτ of the tested models on the area of the shields.

The values of the size of the shields are related to the diameter of the midsection, the total area of the shields is related to the area of the midsection.

Conclusion

A qualitative shadow picture of the flow spectra of the model with aft shields helps to visually link the effectiveness of the controls used with changes in its aerodynamic characteristics. The experimental flow pattern is only qualitatively modeled by numerical calculation and continues to be the best method of verifying a specific package designed for scientific visualization of supersonic flows. The influence of the change in the number of brake shields on the coefficient of the resistance force of the cylindrical-conical model is given.

The work was carried out with the financial support of the Russian Science Foundation (project No. 20-19-00613).

References

1. S.I. Gerasimov, V.I. Erofeev, I.I. Kanygin, A.V. Salnikov Vizualizazia dulnogo vychlopaa pri vystrele iz legkogazovoi pyshki [Visualization of muzzle exhaust following the light gas gun shot] Scientific Visualization, q.2, v.6, №2, 2014
2. S.I. Gerasimov I.I. Kanygin, V.A. Kikeev, V.I. Erofeev., A.P.Fomkin Vizualizazia sverchzvukovogo obtekania fragmentov kubicheskoi formy [Visualization of supersonic flow around cube shaped fragments] Scientific Visualization, q.2, v.7, №3, 2015, pp.12-20
3. S.I. Gerasimov, V.A. Kikeev , K.V. Totyshev, A.P. Fomkin Vizualizazia sverchzvukovogo dvizhenia sfery v vozdyche I v vode [Visualization of supersonic motion of a sphere in air and water] Scientific Visualization, 2017, q.1, №1, v. 9 pp.1-25
4. S.I. Gerasimov, A.V. Zubankov, V.A. Kikeev, I.Yu. Smirnov, N.A. Trepalov Issledovanie charactera otrazhenia v modelnych opytach pryamotenevym metodom vizualizazii [Investigation of wave reflection with shadow technique] Scientific Visualization, 2018, q.4, v.10, №5, pp.98-109
5. S.I. Gerasimov, V.A. Kikeev, V.A. Kuzmin, K.V. Totyshev, A.P. Fomkin Tenevaya shema s selektivnym diapazonom photoregistrazii v aerodinamicheskich ispytaniyach [Shadow scheme with selective range of photoregistration in aerodynamic tests] Scientific visualization, 2019, v. 11, N 2, pp. 1 – 10
6. S.I. Gerasimov, V.I. Erofeev, V.A. Kikeev, K.V. Totyshev, E.G. Kosyak, P.G. Kuznetsov O razvitii techniki aeroballisticheskogo eksperimenta dlya vizualizazii techenii [On the development of aeroballistic experiment techniques for flow visualization] Scientific Visualization 2021, v 13, N 1, pp. 69 – 82
7. S.I. Gerasimov, V.I. Erofeev, E.G. Kosyak Postanovka opytov dlya analiza vozmuhenii golovnoi udarnoi volny za chet prisutstvia chastiz v sverchzvukovom potoke [Setting up experiments for analyzing disturbances of the head shockwave due to the presence of particles in the supersonic flow] Vestnik MSTU by N.E. Bauman, ser. Natural science, №1, 2021, pp.34-46
8. S.I. Gerasimov, V.I. Erofeev, P.G. Kuznetsov, E.G. Kosyak, I.Yu. Smirnov Dvizhenie zatuplennogo cilindra so stabilizatorami po rezultatam aeroballisticheskogo eksperimenta [Motion characteristics of a blunted cylinder with stabilizers according to the results of aeroballistic experiment] TsAGI Science Journal 51(4):355–363 (2020) Volume 51, Issue 4, 2020, pp.355-363
9. S.I. Gerasimov, V.I. Erofeev, M.I. Krutik, K.V. Totyshev, E.G. Kosyak, P.G. Kuznetsov Apparatnyi kompleks, realizuyushii chemy odnovremennogo polucheniya izobrazhenia bystroprotekayushego prozessa v otrazennom I prochodyachem svete [A Hardware Complex Using a Scheme for Simultaneously Obtaining the Image of a Rapid Process in Reflected and Passing Light] Instruments and Experimental Techniques, 2020, No. 5, pp. 88-91© Pleiades Publishing, Ltd., 2020
10. S.I. Gerasimov, M.I. Krutik, V.S. Rozhentsov, A.G. Sirotkina, K.V. Totyshev Registracia bystroprotekayushich prozessov skorostnoi kameroi NANOGATE -22/16 [Imaging Fast Processes Using a NANOGATE-22/16 High-Speed Camera] Instruments and Experimental Techniques, 2022, Vol. 65, No. 3, pp. 509–513. © Pleiades Publishing, Ltd., 2022
11. V.T. Kalugin. Ae`rogazodinamika organov upravleniya poletom letatel`ny`x apparatov. [Aerogasodynamics of flight controls of aircraft.] Textbook. -M.; Publishing house of Bauman Moscow State Technical University, 2004, pp.688.
12. Pogosyan M.A., Savelevskikh E.P., Shagaliev R.M., Kozelkov A.S., Strelets D.Yu., Ryabov A.A., Kornev A.V., Deryugin Yu.N., Spiridonov V.F., Tsiberev K.V. Primenenie otechestvenny`x superkomp`yuterny`x texnologij dlya sozdaniya perspektivny`x obrazczov aviacionnoj texniki. [Application of domestic supercomputer technologies for the creation of promising samples of aviation equipment] // Journal VANT, ser. Mathematical Modeling of Physical Processes, 2013, issue 2, pp.3-18.
13. S.I. Gerasimov, Yu.I. Faykov, S.A. Kholin. Kumulyativny`e istochniki sveta. [Cumulative light sources]. Sarov, 2011, pp. 326.